# REPORT DOCUMENTATION PAGE

Form Approved OMB NO. 0704-0188



| 1. REPORT DATE (DD-MM-YYYY) | 2. REPORT TYPE | 3. DATES COVERED (From - To) |
|---|---|---|
| 05-06-2017 | Final Report | 9-May-2016 - 8-Mar-2017 |

**4. TITLE AND SUBTITLE**
Final Report: Koopman Mode Decomposition: Revisiting the Route to Turbulence

**5a. CONTRACT NUMBER**
W911NF-16-1-0312

**5b. GRANT NUMBER**

**5c. PROGRAM ELEMENT NUMBER**
111111

**6. AUTHORS**
Maria Fonoberova, Igor Mezic, James Hogg

**5d. PROJECT NUMBER**

**5e. TASK NUMBER**

**5f. WORK UNIT NUMBER**

**7. PERFORMING ORGANIZATION NAMES AND ADDRESSES**
AIMdyn, Inc
1919 State St, suite 207

Santa Barbara, CA 93101 -8455

**8. PERFORMING ORGANIZATION REPORT NUMBER**

**9. SPONSORING/MONITORING AGENCY NAME(S) AND ADDRESS (ES)**
U.S. Army Research Office
P.O. Box 12211
Research Triangle Park, NC 27709-2211

**10. SPONSOR/MONITOR'S ACRONYM(S)**
ARO

**11. SPONSOR/MONITOR'S REPORT NUMBER(S)**
68731-EG.3

**12. DISTRIBUTION AVAILIBILITY STATEMENT**
Approved for Public Release; Distribution Unlimited

**13. SUPPLEMENTARY NOTES**
The views, opinions and/or findings contained in this report are those of the author(s) and should not contrued as an official Department of the Army position, policy or decision, unless so designated by other documentation.

**14. ABSTRACT**
The purpose of the proposed project was to continue the approach we have developed, with ARO support, in collaboration with ARL and Dr. Bryan Glaz, pursue a deeper study of transition to turbulence we have observed and extend it to shed the light on classical theories of turbulence. The proposed work is fundamental for developing better understanding of transition phenomena that has so far eluded theoretical description using low order models, and more generally for understanding dynamical systems phenomena that occur in systems that are being periodically forced through a Hopf and other oscillatory bifurcations.

**15. SUBJECT TERMS**
Koopman mode analysis, oscillating cylinder flow, proper orthogonal decomposition, normal form

| 16. SECURITY CLASSIFICATION OF: | | | 17. LIMITATION OF ABSTRACT | 15. NUMBER OF PAGES | 19a. NAME OF RESPONSIBLE PERSON |
|---|---|---|---|---|---|
| a. REPORT | b. ABSTRACT | c. THIS PAGE | | | Maria Fonoberova |
| UU | UU | UU | UU | | 19b. TELEPHONE NUMBER 805-687-6999 |

## Report Title

Final Report: Koopman Mode Decomposition: Revisiting the Route to Turbulence

## ABSTRACT

The purpose of the proposed project was to continue the approach we have developed, with ARO support, in collaboration with ARL and Dr. Bryan Glaz, pursue a deeper study of transition to turbulence we have observed and extend it to shed the light on classical theories of turbulence. The proposed work is fundamental for developing better understanding of transition phenomena that has so far eluded theoretical description using low order models, and more generally for understanding dynamical systems phenomena that occur in systems that are being periodically forced through a Hopf and other oscillatory bifurcations.

In this project, in collaboration with Dr. Bryan Glaz, we analyzed fluid dynamics induced by periodically forced flow around a cylinder for the case when the forcing frequency is much lower than the von Karman vortex shedding frequency corresponding to the constant flow velocity condition. By using the Koopman Mode Decomposition approach, we found a new normal form equation that extends the classical Hopf bifurcation normal form by a time-dependent term for Reynolds numbers close to the Hopf bifurcation value. The normal form describes the dynamics of an observable and features a forcing (control) term that multiplies the state, and is thus a parametric - i.e. not an additive - forcing effect. We found that the dynamics of the flow in this regime are characterized by alternating instances of quiescent and strong oscillatory behavior, and that this pattern persists indefinitely. Furthermore, the spectrum of the associated Koopman operator possesses quasi-periodic features. We established the theoretical underpinnings of this phenomenon -- that we name Quasi-Periodic Intermittency -- using the new normal form model and showed that the dynamics are caused by the tendency of the flow to oscillate between the unstable fixed point and the stable limit cycle of the unforced flow. The quasi-periodic intermittency phenomena is also characterized by positive Finite-Time Lyapunov Exponents that, over a long period of time, asymptotically approach zero. We have also worked on the comparison between the POD and KMD analysis and the normal form equation control.

---

## Enter List of papers submitted or published that acknowledge ARO support from the start of the project to the date of this printing. List the papers, including journal references, in the following categories:

### (a) Papers published in peer-reviewed journals (N/A for none)

| Received | Paper |
|---|---|
| 06/05/2017 | 2 Bryan Glaz, Igor Mezic, Maria Fonoberova, Sophie Loire. Quasi-Periodic Intermittency in Oscillating Cylinder Flow, Journal of Fluid Mechanics, ( ): . doi: |
| | 1,043,277.00 |
| **TOTAL:** | **1** |

**Number of Papers published in peer-reviewed journals:**

---

### (b) Papers published in non-peer-reviewed journals (N/A for none)

| Received | Paper |
|---|---|
| **TOTAL:** | |

**Number of Papers published in non peer-reviewed journals:**

## (c) Presentations

**Number of Presentations:** 0.00

### Non Peer-Reviewed Conference Proceeding publications (other than abstracts):

| Received | Paper |
|---|---|

**TOTAL:**

**Number of Non Peer-Reviewed Conference Proceeding publications (other than abstracts):**

### Peer-Reviewed Conference Proceeding publications (other than abstracts):

| Received | Paper |
|---|---|

**TOTAL:**

**Number of Peer-Reviewed Conference Proceeding publications (other than abstracts):**

## (d) Manuscripts

| Received | Paper |
|---|---|

**TOTAL:**

**Number of Manuscripts:**

## Books

Received Book

**TOTAL:**

Received Book Chapter

**TOTAL:**

## Patents Submitted

## Patents Awarded

## Awards

## Graduate Students

| NAME | PERCENT_SUPPORTED |
|---|---|
| **FTE Equivalent:** | |
| **Total Number:** | |

## Names of Post Doctorates

| NAME | PERCENT_SUPPORTED |
|---|---|
| **FTE Equivalent:** | |
| **Total Number:** | |

## Names of Faculty Supported

| NAME | PERCENT_SUPPORTED |
|---|---|

**FTE Equivalent:**
**Total Number:**

## Names of Under Graduate students supported

| NAME | PERCENT_SUPPORTED |
|---|---|

**FTE Equivalent:**
**Total Number:**

## Student Metrics

This section only applies to graduating undergraduates supported by this agreement in this reporting period

| | |
|---|---|
| The number of undergraduates funded by this agreement who graduated during this period: ..... | 0.00 |
| The number of undergraduates funded by this agreement who graduated during this period with a degree in science, mathematics, engineering, or technology fields:..... | 0.00 |
| The number of undergraduates funded by your agreement who graduated during this period and will continue to pursue a graduate or Ph.D. degree in science, mathematics, engineering, or technology fields:..... | 0.00 |
| Number of graduating undergraduates who achieved a 3.5 GPA to 4.0 (4.0 max scale):..... | 0.00 |
| Number of graduating undergraduates funded by a DoD funded Center of Excellence grant for Education, Research and Engineering:..... | 0.00 |
| The number of undergraduates funded by your agreement who graduated during this period and intend to work for the Department of Defense ..... | 0.00 |
| The number of undergraduates funded by your agreement who graduated during this period and will receive scholarships or fellowships for further studies in science, mathematics, engineering or technology fields: ..... | 0.00 |

## Names of Personnel receiving masters degrees

| NAME |
|---|

**Total Number:**

## Names of personnel receiving PHDs

| NAME |
|---|

**Total Number:**

## Names of other research staff

| NAME | PERCENT_SUPPORTED |
|---|---|
| Maria Fonoberova | 0.60 |
| Igor Mezic | 0.30 |
| James Hogg | 0.10 |
| **FTE Equivalent:** | **1.00** |
| **Total Number:** | **3** |

## Sub Contractors (DD882)

## Inventions (DD882)

## Scientific Progress

See Attachment

## Technology Transfer

# Final Report
# Proposal Number: 68731EG
# Agreement Number: W911NF1610312
# Proposal Title: Koopman Mode Decomposition: Revisiting the Route to Turbulence
# Report Period Begin Date: 05/09/2016
# Report Period End Date: 03/08/2017
# PI: Dr. Maria Fonoberova

CONTENTS



## 1. Introduction

The purpose of the proposed project was to continue the approach we have developed, with ARO support, in collaboration with ARL and Dr. Bryan Glaz, pursue a deeper study of transition to turbulence we have observed and extend it to shed the light on classical theories of turbulence. The proposed work is fundamental for developing better understanding of transition phenomena that has so far eluded theoretical description using low order models, and more generally for understanding dynamical systems phenomena that occur in systems that are being periodically forced through a Hopf and other oscillatory bifurcations.

In this project, in collaboration with Dr. Bryan Glaz, we analyzed fluid dynamics induced by periodically forced flow around a cylinder for the case when the forcing frequency is much lower than the von Kármán vortex shedding frequency corresponding to the constant flow velocity condition. By using the Koopman Mode Decomposition approach, we found a new normal form equation that extends the classical Hopf bifurcation normal form by a time-dependent term for Reynolds numbers close to the Hopf bifurcation value. The normal form describes the dynamics of an observable and features a forcing (control) term that multiplies the state, and is thus a parametric - i.e. not an additive - forcing effect. We found that the dynamics of the flow in this regime

are characterized by alternating instances of quiescent and strong oscillatory behavior, and that this pattern persists indefinitely. Furthermore, the spectrum of the associated Koopman operator possesses quasi-periodic features. We established the theoretical underpinnings of this phenomenon – that we name Quasi-Periodic Intermittency – using the new normal form model and showed that the dynamics are caused by the tendency of the flow to oscillate between the unstable fixed point and the stable limit cycle of the unforced flow. The quasi-periodic intermittency phenomena is also characterized by positive Finite-Time Lyapunov Exponents that, over a long period of time, asymptotically approach zero. We have also worked on the comparison between the POD and KMD analysis and the normal form equation control.

## 2. Cylinder Flow

Two-dimensional CFD simulations of a streamwise oscillating circular cylinder were considered. For the stationary cylinder, the system can be expressed in the general dynamical systems form given by

$$\dot{\mathbf{z}} = \mathbf{F}(\mathbf{z}), \tag{2.1}$$

where $\mathbf{z}$ is the vector of streamwise and transverse velocity components in the discretized domain, and $\mathbf{F}$ are the discretized incompressible Navier-Stokes equations. When the oncoming streamwise flow is oscillated, traditionally the forced Navier-Stokes equations were written in the format

$$\dot{\mathbf{z}} = \mathbf{F}(\mathbf{z}) + B\mathbf{u}(t). \tag{2.2}$$

where $B$ is a linear operator. ln the problem considered here the forcing can enter via boundary conditions, and thus the forcing does not necessarily affect all the states in structurally the same way. Thus, as we show below, $B$ is not necessarily state-independent.

Similar to the implementation described in Perdikaris *et al.* (2009), at the domain inlet boundary, the elements of $B\mathbf{u}$ are $2q\sin(\omega_f t)$ for the streamwise velocity components, and 0 for the transverse components. Furthermore, $\mathbf{F}(\mathbf{z}) = 0$ is at the inlet boundary. At all other locations in the domain away from the inlet boundary, $B = 0$. The amplitude of the oscillation is controlled by $q$, and the prescribed frequency is $\omega_f = 2\pi f$.

As in Leontini *et al.* (2013), the CFD equations are solved in a frame of reference attached to the moving cylinder. Therefore, the resultant oncoming streamwise flow velocity $u_\infty$ over the cylinder is

$$u_\infty(t) = u_0 - \frac{2q}{\omega_f}\cos\left(\omega_f t\right), \tag{2.3}$$

where $u_0$ is the steady component of the freestream. Since sinusoidal cylinder motions are prescribed, the oscillatory Reynolds number $Re$ is

$$Re(t) = Re_0 - Re_q \sin\left(\omega_f t\right), \tag{2.4}$$

where $Re_0 = u_0 D/\nu$, $Re_q = 2qD/(\omega_f \nu)$, $\nu$ is the kinematic viscosity, and $D$ is the cylinder diameter. The commercial software package, CFD++ was used for all CFD solutions of (2.1) and (2.2). The CFD++ framework is a finite-volume based solver and is second order accurate in space. Implicit, dual time-stepping was employed.

The connections between Hopf bifurcation dynamics and flow past a stationary cylinder are well known (Sreenivasan *et al.* 1987). In such systems, a critical Hopf bifurcation parameter $\mu$ exists such that:

- For $\mu < 0$: perturbations to the system decay.

• For $\mu = 0$: the system is neutrally stable and initial perturbations induce oscillations that neither decay nor grow.

• For $\mu > 0$: initial perturbation amplitudes grow in a transient manner until reaching a saturation value; the system is characterized by limit cycle oscillations for long time.

The Hopf bifurcation limit cycle frequency corresponds to the von Kármán wake shedding mode and $\mu$ is proportional to $(Re_0 - Re_c)$, where $Re_c$ is the critical value at which vortex shedding initiates (Sreenivasan *et al.* 1987). Without loss of generality, we consider the critical bifurcation value to be $\mu = \mu_0 = 0$. These dynamics can be expressed by the classical Landau equation (i.e. first-order normal form equation),

$$\dot{\eta} = \lambda_1(\mu)\eta + \beta(\mu)\eta^2\bar{\eta}, \tag{2.5}$$

where $\eta$ represents a time-dependent state governed by the bifurcation dynamics (e.g. velocity in the cylinder wake, integrated lift force, etc.), $\lambda_1(\mu)$ is complex valued such that $\Im[\lambda_1(\mu)]$ corresponds to the von Kármán wake shedding frequency, $\Re[\lambda_1(\mu)]$ is the associated growth/decay rate, and $\beta(\mu)$ is a complex valued parameter that effects the limit cycle saturation amplitude and frequency. Identification of the parameters in (2.5) as functions of $Re_0$ for stationary cylinder wake shedding was established by Sreenivasan *et al.* (1987). In the following sections, we extend the standard Hopf bifurcation normal form (2.5) to account for the effects of forcing.

## 3. Koopman Mode Decomposition

A summary of Koopman modal analysis is provided in this section. The modal analysis stems from a decomposition of an infinite linear dimensional operator that captures the dynamics of an arbitrary observable functional, even if the observable is a nonlinear function of a dynamical system state. By utilizing such an approach, the dynamics of some measurable quantity can be described directly and without linearization of the underlying dynamical system. Additional details can be found in Mezić (2013).

### 3.1. *Continuous time*

For the general dynamical system (2.1) defined on a state-space $A$ (i.e. $\mathbf{z} \in A$), where $\mathbf{z}$ is a $\mathbb{R}^{\mathrm{N}}$ vector and $\mathbf{F}$ is a possibly nonlinear vector-valued function of the same dimension as its argument $\mathbf{z}$. We denote by $\mathbf{S}^t(\mathbf{z}_0)$ the position at time $t$ of a trajectory corresponding to (2.1) that starts at initial condition $\mathbf{z}_0$.

An arbitrary vector-valued observable from $A$ to $\mathbb{R}^p$ is denoted by $\mathbf{g}$. The value of $\mathbf{g}$ at time $t$ starting from the system trajectory initial condition $\mathbf{z}_0$ is

$$\mathbf{g}(t, \mathbf{z}_0) = \mathbf{g}(\mathbf{S}^t(\mathbf{z}_0)). \tag{3.1}$$

Note that the space of observables $\mathbf{g}$ is a vector space. The family of operators $U^t$, acting on the space of observables parameterized by time $t$ is defined by

$$U^t\mathbf{g}(\mathbf{z}_0) = \mathbf{g}(\mathbf{S}^t(\mathbf{z}_0)). \tag{3.2}$$

Thus, for a fixed time $\tau$, $U^\tau$ maps the vector-valued observable $\mathbf{g}(\mathbf{z}_0)$ to $\mathbf{g}(\tau, \mathbf{z}_0)$. With some abuse of language we will call the family of operators $U^t$ the Koopman operator of the continuous-time system given by Eqn. (2.1). This operator was defined for the first time in Koopman (1931), for Hamiltonian systems. In operator theory, such operators, when defined for general dynamical systems, are often called composition operators, since $U^t$ acts on observables by composing them with the mapping $\mathbf{S}^t$ (Singh & Manhas 1993).

The operator $U^t$ is linear as can be easily seen from its definition by Eqn. (3.2), and thus

it makes sense to consider its spectral properties in the context of analyzing Eqn. (2.1). In this direction, we will be looking for special observables $\phi(\mathbf{z}) : A \to \mathbb{C}$ on the state space that have the evolution in time given by

$$U^t\phi(\mathbf{z}_0) = \phi(\mathbf{S}^t(\mathbf{z}_0)) = \exp(\lambda t)\phi(\mathbf{z}_0).$$

Such observables (functions) $\phi$ are the eigenfunctions of $U^t$, and the associated complex numbers $\lambda$ are the eigenvalues of $U^t$.

For quasi-periodic attractors, the observables can be expanded onto a basis system spanned by the Koopman eigenfunctions as (Mezić 2005, 2013)

$$\mathbf{g}(t, \mathbf{z}_0) = \sum_{j=1}^{\infty} \phi_j(\mathbf{z})\mathbf{s}_j = \sum_{j=1}^{\infty} U^t\phi_j(\mathbf{z}_0)\mathbf{s}_j = \sum_{j=1}^{\infty} e^{\lambda_j t}\mathbf{v}_j(\mathbf{z}_0) + e^{\bar{\lambda}_j t}\bar{\mathbf{v}}_j(\mathbf{z}_0), \tag{3.3}$$

where $\mathbf{s}_j$ are the Koopman modes and represent the projections of the observables onto the eigenfunctions, $\mathbf{v}(\mathbf{z}_0) = \phi_j(\mathbf{z}_0)\mathbf{s}_j$, and $\bar{\lambda}_j$, $\bar{\mathbf{v}}_j$ are the complex conjugates of $\lambda_j$ and $\mathbf{v}_j$ respectively.

### 3.2. *Discrete time and computation of Koopman modes*

Due to the discrete nature of numerical simulations or experimental data, the dynamical system can be described by a discrete sequence of state values or observables:

$$\mathbf{z}_{k+1} = \mathbf{F}(\mathbf{z}_k)$$

and a discrete sequence of $U^{k\Delta t};\ k = 0; \cdots; N$ is obtained. It is easy to show that the discrete version of (3.3) is (Mezić 2005, 2013)

$$\mathbf{g}(\mathbf{z}_k) = \sum_{j=1}^{\infty} \phi_j(\mathbf{z}_k)\mathbf{s}_j = \sum_{j=1}^{\infty} U^k\phi_j(\mathbf{z}_0)\mathbf{s}_j = \sum_{j=1}^{\infty} \lambda_j^k\mathbf{v}_j(\mathbf{z}_0) + \bar{\lambda}_j^k\bar{\mathbf{v}}_j(\mathbf{z}_0). \tag{3.4}$$

Koopman modes can in principle be computed directly based on snapshots of the flow, using the Generalized Laplace Analysis (Mezić 2013). The Koopman Modes can also be approximated by using an Arnoldi-like algorithm (Schmid & Sesterhenn 2008; Rowley *et al.* 2009) which computes eigenvalues based on the so-called companion matrix.

Given a sequence of equispaced in time snapshots from numerical simulations or physical experiments, with $\Delta t$ being the time interval between snapshots, a data matrix is formed, columns of which represent the individual data samples $u_j \in \mathbb{R}^n,\ j = 0; \cdots; m$ with $j$ representing time $j\Delta t$. The companion matrix is then defined as:

$$C = \begin{pmatrix} 0 & 0 & \cdots & 0 & c_0 \\ 1 & 0 & & 0 & c_1 \\ 0 & 1 & & 0 & c_2 \\ \vdots & & \ddots & & \vdots \\ 0 & 0 & \cdots & 1 & c_{m-1} \end{pmatrix} \tag{3.5}$$

where $c_i,\ i = 0, \cdots, m-1$ are such that:

$$u_m = \sum_{j=0}^{m-1} c_i u_i + r$$

and $r$ is the residual vector.

The spectrum of the Koopman operator restricted to the subspace spanned by $u_j$ is equal to the spectrum of the infinite-dimensional companion matrix and the associated

Koopman modes are given by $Ka$ (provided that $a$ does not belong to the null space of K), where $K = [u_0;\ u_1 \cdots ;\ u_{m-1}]$ is the column matrix (vector-valued) of observables snapshots at times $0; \Delta t; \cdots ; (m-1)\Delta t$ and $a$ is an eigenvector of the shift operator restricted to Krylov subspace spanned by $u_i$ which the companion matrix is an approximation of. The approximate Koopman eigenvalues and eigenvectors obtained by the Arnoldi's algorithm are sometimes called Ritz eigenvalues and eigenvectors.

The standard Arnoldi-type algorithm to calculate the Ritz eigenvalues $\beta_j$ and eigenfunctions $v_j$ is as follows:

(i) Define $K = [u_0, u_1, \cdots, u_{m-1}]$.

(ii) Find constants $c_j$ such that:

$$r = u_m - \sum_{j=0}^{m-1} c_j u_j = u_m - Kc,\ r \perp span\{u_0, ..., u_{m-1}\}.$$

This can be done by defining $c = K^+ u_m$ where $K^+$ is the pseudo inverse of $K$.

(iii) Define the companion matrix $C$ by Eqn. (3.5) and find its eigenvalues and eigenvectors:

$$C = T^{-1} \alpha T, \alpha = diag(\alpha_1, \cdots, \alpha_m),$$

where eigenvectors are columns of $T^{-1}$. Note that the Vandermonde matrix, $\tilde{T}$:

$$\tilde{T} = \begin{pmatrix} 1 & \alpha_1 & \alpha_1^2 & \cdots & \alpha_1^{m-1} \\ 1 & \alpha_2 & \alpha_2^2 & \cdots & \alpha_2^{m-1} \\ \vdots & \vdots & \vdots & \ddots & \vdots \\ 1 & \alpha_m & \alpha_m^2 & \cdots & \alpha_m^{m-1} \end{pmatrix}$$

diagonalizes the companion matrix $C$ , as long as the eigenvalues $\alpha_1, \cdots, \alpha_m$ are distinct.

(iv) Define $v_j$ to be the columns of $V = K\tilde{T}^{-1}$.

Then, the Arnoldi-type Koopman Mode Decomposition gives:

$$\forall k = [0, 1, \cdots, m],\ u_k = \sum_{j=1}^{m} \alpha_j^k V(:, j).$$

To fairly compare the contribution of all the Koopman modes, the eigenvectors of the companion matrix $C$ can be normalized to be unitary i.e the column of $T^{-1}$ are normalized to have norm 1. Let $N_j = \|T^{-1}(:, j)\|$ and $V_N(:, j) = KT^{-1}(:, j)/N_j$, then:

$$\forall k = [0, 1, \cdots, m],\ u_k = \sum_{j=1}^{m} \alpha_j^k V_N(:, j) N_j. \tag{3.6}$$

## 4. Dynamics of Observables with Applied Forcing

The evolution of an observable function of interest subject to applied forcing is developed in this section. The full-order representations are derived first, which explicitly show how forcing effects appear in the dynamics-of-observables equations. In order to obtain a lower order representation that can be used to understand phenomena observed in the forced bifurcation systems, projections onto the unforced system Koopman shedding mode basis are described. This basis corresponds to the center manifold of the unforced system. Finally, the nonlinearity in the reduced-order equations are simplified further for $f << f_0$ to obtain remarkably simple mathematical model equations that explain the salient features of the seemingly complex dynamical states.

### 4.1. *Full Order Equations*

Considering the observables evolved by the Koopman operator as in (3.2), we denote

$$\mathbf{g}(t, \mathbf{z}_0) = \mathbf{g}(S^t \mathbf{z}_0).$$

Note that $\mathbf{g}(t, \mathbf{z}_0)$ depends on the initial condition $\mathbf{z}_0$ so we can think of it as a function in the Lagrangian frame - but in the state space, not in the physical space! We have

$$\begin{aligned} \frac{\partial \mathbf{g}(t, \mathbf{z}_0)}{\partial t} &= \frac{\partial \mathbf{g}(S^t \mathbf{z}_0)}{\partial t} = \nabla \mathbf{g}(S^t \mathbf{z}_0)) \cdot \frac{\partial S^t \mathbf{z}_0}{\partial t} \\ &= \dot{\mathbf{z}} \cdot \nabla \mathbf{g}(t, \mathbf{z}_0) = \mathbf{F}(\mathbf{z}) \cdot \nabla \mathbf{g}(t, \mathbf{z}_0) \end{aligned} \tag{4.1}$$

where (2.1) has been substituted for $\dot{\mathbf{z}}$ and the gradient operator corresponds to the state space. Equation (4.1) describes the evolution of observables starting from a smooth initial condition given by $\mathbf{g}(0, \mathbf{z}_0)$. In operator form, (4.1) can be written as

$$\frac{\partial \mathbf{g}}{\partial t} = (\mathbf{F} \cdot \nabla)\, \mathbf{g} = L\mathbf{g}, \tag{4.2}$$

where $L$ is the linear infinite dimensional operator - the generator of Koopman operator evolution - that fully characterizes the evolution of $\mathbf{g}$, which can be a nonlinear function of $\mathbf{z}$. From (4.2), the Koopman operator is given by

$$U^t = e^{Lt}. \tag{4.3}$$

The linkages between the Landau equation (2.5) and the Koopman operator (4.3) for post-critical flow past a stationary cylinder were established in Bagheri (2013).

Now, an applied forcing $B\mathbf{u}(t)$, where $B$ is a linear operator, and $\mathbf{u}$ is a vector in the same space as $\mathbf{z}$, can be added to the Navier-Stokes equations, as in (2.2). Substituting the forced system (2.2) into (4.1) leads to

$$\frac{\partial \mathbf{g}(t, \mathbf{z}_0)}{\partial t} = (\mathbf{F}(\mathbf{z}) + B\mathbf{u}(t)) \cdot \nabla \mathbf{g}(t, \mathbf{z}_0) = L\mathbf{g} + (B\mathbf{u} \cdot \nabla)\, \mathbf{g}. \tag{4.4}$$

Although the external forcing in the underlying system (2.2) appears as an additive term, it is clear from (4.4) that forcing appears as a bi-linear term in $\mathbf{g}$ and $\mathbf{u}$ when considering the time evolution of a general observable. Similarly, it is clear from (4.4) that additive forcing can only occur when considering dynamics-of-observables in the special case when $\mathbf{g}$ is a linear function of $\mathbf{z}$. Therefore, the original additive forcing will lead to a parametric type excitation in the observable evolution equation for the general case when $\mathbf{g}$ is a nonlinear function of $\mathbf{z}$. Note that the forcing $\mathbf{u}$ could also be thought of as a control input; thus (4.4) also demonstrates that control studies involving dynamics-of-observables models based on additive forcing in the underlying system must involve a term multiplicative in control $\mathbf{u}$, which in the simplest case reduces to a bi-linear term.

### 4.2. *Koopman Modes and the Unforced System Reduced-Order Model*

In the vicinity of a non-hyperbolic fixed point in state space, the long-time behavior can be accurately represented by the dynamics on the lower dimensional center manifold (Wiggins 1990). Therefore, we truncate the projection in (3.3) by considering a subspace spanned by the Koopman eigenfunction and eigenvalue corresponding to $\Re[\lambda_j(\mu_0)] = 0$ and $\Im[\lambda_j(\mu_0)] = \omega_0(\mu_0) \neq 0$. For flow over a stationary cylinder, this is the well known von Kármán wake shedding (bifurcation) mode. If the Koopman eigensolutions are ordered such that $j = 1$ is the bifurcation mode, then (3.3) is approximated by the truncated expansion

$$\mathbf{g}(t, \mathbf{z}_0) \approx \gamma_1(t)\mathbf{v}_1(\mathbf{z}_0) + \bar{\gamma_1}(t)\bar{\mathbf{v}}_1(\mathbf{z}_0) = \mathbf{V}\boldsymbol{\Gamma}, \tag{4.5}$$

where $\mathbf{V} = [\mathbf{v}_1, \bar{\mathbf{v}}_1] \in \mathbb{C}^{p\times 2}$, and $\boldsymbol{\Gamma} = [\gamma_1, \bar{\gamma}_1]^T \in \mathbb{C}^{2\times 1}$ contains the the complex valued time-dependent coefficients $\gamma_1$ and $\bar{\gamma}_1$ which replace the exponential terms when considering reduced-order approximations (Susuki & Mezić 2012). Substituting (4.5) into (4.1) and noting that $\mathbf{z} = \mathbf{g}^{-1}(\mathbf{g}(\mathbf{z}))$ leads to the reduced-order model,

$$\dot{\boldsymbol{\Gamma}} = \left(\mathbf{V}^\dagger\mathbf{V}\right)^{-1}\mathbf{V}^\dagger\left[\mathbf{F}\circ\mathbf{g}^{-1}\left(\mathbf{g}\left(\mathbf{V}\boldsymbol{\Gamma}\right)\right)\cdot\nabla\left(\mathbf{V}\boldsymbol{\Gamma}\right)\right]. \tag{4.6}$$

This two-dimensional reduced-order model can be re-written as

$$\begin{bmatrix} \dot{\gamma}_1 \\ \dot{\bar{\gamma}}_1 \end{bmatrix} = \begin{bmatrix} \lambda_1(\mu) & 0 \\ 0 & \bar{\lambda}_1(\mu) \end{bmatrix}\begin{bmatrix} \gamma_1 \\ \bar{\gamma}_1 \end{bmatrix} + \hat{\mathbf{F}}(\gamma_1, \bar{\gamma}_1, \mu) \tag{4.7}$$

where the right-hand side of (4.6) has been expressed as a linear term plus a nonlinear term, i.e.

$$\left(\mathbf{V}^\dagger\mathbf{V}\right)^{-1}\mathbf{V}^\dagger\left[\mathbf{F}\circ\mathbf{g}^{-1}\left(\mathbf{g}\left(\mathbf{V}\boldsymbol{\Gamma}\right)\right)\cdot\nabla\left(\mathbf{V}\boldsymbol{\Gamma}\right)\right] = \begin{bmatrix} \lambda_1(\mu) & 0 \\ 0 & \bar{\lambda}_1(\mu) \end{bmatrix}\begin{bmatrix} \gamma_1 \\ \bar{\gamma}_1 \end{bmatrix} + \hat{\mathbf{F}}(\gamma_1, \bar{\gamma}_1, \mu). \tag{4.8}$$

Equation (4.7) can be thought of as the projection of (4.1) onto the center manifold spanned by the basis corresponding to the primary Koopman shedding (bifurcation) mode at $\mu = \mu_0$. Since $\gamma_1$ and $\bar{\gamma}_1$ in (4.7) correspond to complex conjugate states, it is sufficient to solve one of the complex valued differential equations,

$$\dot{\gamma}_1 = \lambda_1(\mu)\gamma_1 + \hat{F}_1(\gamma_1, \bar{\gamma}_1, \mu), \tag{4.9}$$

where $\hat{F}_1$ is the first element of the vector $\hat{\mathbf{F}}$. It is important to note that, (4.7) - (4.9) are expressed as functions of the bifurcation parameter $\mu$, even though the reduced order projections are based on the Koopman modes at $\mu = \mu_0$. This is valid for values of $\mu$ in the vicinity of $\mu_0$ for dynamics projected onto the center manifold; i.e. the Koopman modes at $\mu = \mu_0$ are a valid projection basis for all values of $\mu$ in the vicinity of $\mu_0$ since the orbit of the full order system (4.2) near $\mu_0$ is determined by the solution restricted to the center manifold (Wiggins 1990).

### 4.3. *Koopman Modes and the Forced System Reduced-Order Model*

The appropriate basis for model order reduction of the forced Hopf bifurcation system is considered next. We make the argument that the unforced Koopman modes at the Hopf bifurcation value of the Reynolds number (i.e. $\mu = \mu_0$) can be used as the projection bases, even for the forced system. From (4.4), the dynamics of the forced system are described by the unforced linear operator $L$ plus an additional time-variant forcing term that is bi-linear in $\mathbf{u}$ and $\mathbf{g}$. We know that the unforced Koopman eigenvalues and eigenfunctions satisfy

$$L\phi_i(\mathbf{z}) = \lambda_i\phi_i(\mathbf{z}), i = 0, 1, 2, \ldots, \infty. \tag{4.10}$$

As a result, if we select a basis spanned by unforced system Koopman eigenfunctions, as in (3.3), then the full action of $L$ on $\mathbf{g}$ in (4.4) will be captured. If the forcing term is properly projected onto the new basis, then $\dot{\mathbf{g}}$ will be represented without any approximation. Therefore, the modes computed from the unforced system can be used as an appropriate basis for model order reduction of the forced system. This implies that the spatial modal structures of the unforced bifurcation system persist into the forced case, though the corresponding time dependence $\gamma_1(t)$ will differ between the two cases. However, just as in the case for the unforced reduced-order model, truncation to a finite number of modes will introduce error. Therefore, one would still need to be careful to include modes that may not be significant in unforced conditions, but become relevant when the forcing is

applied. Since we are primarily interested in the shedding dynamics under forcing, we restrict our projection to just the primary bifurcation mode (and its complex conjugate), just as in the unforced case.

Proceeding with the reduced-order model development for the forced system, the expansion (4.5) is substituted into (4.4), which leads to

$$\begin{bmatrix} \dot{\gamma_1} \\ \dot{\bar{\gamma}_1} \end{bmatrix} = \begin{bmatrix} \lambda_1(\mu) & 0 \\ 0 & \bar{\lambda}_1(\mu) \end{bmatrix} \begin{bmatrix} \gamma_1 \\ \bar{\gamma}_1 \end{bmatrix} + \hat{\mathbf{F}}(\gamma_1, \bar{\gamma_1}, \mu) + \left(\mathbf{V}^\dagger \mathbf{V}\right)^{-1} \mathbf{V}^\dagger \left[\mathbf{u} \cdot \nabla(\mathbf{V}\boldsymbol{\Gamma})\right]. \quad (4.11)$$

In this study, we assume simple harmonic time-dependance for $\mathbf{u}$ with frequency $\omega_f = 2\pi f$. When the elements of $\mathbf{u}$ corresponding to the streamwise velocity components equal $2q\sin(\omega_f t)$, and all other elements equal zero, then

$$\dot{\gamma}_1 = \lambda_1(\mu)\gamma_1 + \hat{F}_1(\gamma_1, \bar{\gamma}, \mu) + 2q\sin(\omega_f t)\left[\gamma_1 a + \bar{\gamma}_1 \bar{a}\right], \quad (4.12)$$

where $a(\mathbf{z}_0)$ corresponds to the first element of the vector $\left(\mathbf{V}^\dagger\mathbf{V}\right)^{-1}\mathbf{V}^\dagger \sum_{i=1}^{N} \partial \mathbf{v}_1/\partial z_i$, and $\bar{a}(\mathbf{z}_0)$ is its complex conjugate. Furthermore, we replace the explicit time dependence in the forcing term by an additional state, $\zeta = e^{i\omega_f t}$ such that (4.12) becomes

$$\dot{\gamma}_1 = \lambda_1(\mu)\gamma_1 + \hat{F}_1(\gamma_1, \bar{\gamma}_1, \mu) - iq(\zeta - \bar{\zeta})\left(\gamma_1 a + \bar{\gamma}_1 \bar{a}\right). \quad (4.13)$$

Note the bi-linear terms involving $\zeta$ and $\gamma_1$ originate from $\mathbf{u} \cdot \nabla \mathbf{g}$ in (4.4).

### 4.4. *Normal Form Theory*

Further simplification of the reduced-order equation (4.13) is possible by eliminating nonlinear terms that are not necessary to retain in the ordinary differential equation. Instead, the eliminated terms can be added after solving the simplified differential equation to obtain the solution for $\gamma_1(t)$. To do this, we applied normal form theory (Guckenheimer & Holmes 1983; Wiggins 1990; Nayfeh 2011). As we will show, normal form theory leads to explicit necessary conditions for the forcing to induce spectral broadening, along with the conditions for which chaos can be ruled out *a priori* as a first order phenomena. We arrived at the following equations that describe time evolution of the amplitude and phase of the unforced shedding Koopman mode:

$$\dot{r} = \sigma(\mu)r + \beta_R(\mu)r^3 + 2rQ_R\sin(\omega_f t) \quad (4.14)$$

and

$$\dot{\theta} = \omega_0(\mu) + \beta_I r^2 + 2Q_I\sin(\omega_f t) \quad (4.15)$$

where $\beta_R$ and $\beta_I$ are the real and imaginary parts of $\beta$. It can be shown that this normal form system is analogous to a nonlinear mechanical oscillator with a parametrically excited damper corresponding to $2Q_R\sin(\omega_f t)$, and a parametrically driven spring stiffness associated with $Q_I\sin(\omega_f t)$. Furthermore, for the range of parameters corresponding to cylinder flow considered in this study, $\omega_0 + \beta_I r^2 >> Q_I$. Thus, the forcing primarily affects the dynamics through the parametrically excited damping. Note that if $\mathbf{g}$ is linear in $\mathbf{z}$, then the forcing would not appear as a radial excitation in (4.14).

Interestingly, a similar set of equations as (4.14) and (4.15) were studied by Wang & Young (2003); Lin & Young (2008) in which it was shown that *shear induced chaos* could be induced. However, a fundamental difference between the shear induced chaos attractor and (4.14) and (4.15) is that the equation governing $\dot{r}$ in (Lin & Young 2008) contained functional dependance on $\theta$ in the bi-linear forcing term. Clearly, this is not the case for (4.14) and leads to different behavior compared to the shear induced chaos attractor. (4.14) and (4.15) do not lead to chaos, and in fact describe a fundamentally different phenomena.

## 5. Quasi-Periodic Intermittency

For the CFD simulations, the cylinder was 0.002 m in diameter and the time step was 1e-4 s. The simulation was run for 60000 time steps, which was sufficient to allow the near-wake dynamics to settle into the well known post-bifurcation limit cycle behavior. The oncoming freestream was $Re_0 = 53$. A low freestream Reynolds number was selected so that turbulence could be neglected. Note that the CFD cylinder simulation exhibited the von Kármán vortex instability at $Re_c = 46$, which is in good agreement with experimental results presented in the literature (Sreenivasan *et al.* 1987). In addition, the calculated vortex shedding frequency at $Re_0 = 53$ was 26 Hz, which is consistent with empirical relations from the literature. For instance, the Roshko number from our simulations is $f_0 D^2/\nu = 7$ at $Re_0 = 53$, which agrees with the empirical relationship from Sreenivasan *et al.* (1987) in which $f_0 D^2/\nu = 5.46 + 0.21\,(Re_0 - Re_c) = 7$. For the oscillating cylinder, the streamwise velocity oscillations were prescribed at $f = 0.5$ Hz for $Re_0 = 53$, which is two orders of magnitude slower than the shedding frequency for the stationary cylinder. As a result of the separation of scales associated with $f << f_0$, we focus on dynamical states other than lock-on/synchronization phenomena that occur when $f \sim f_0$. Oscillation amplitudes from $Re_q = 1$ to $Re_q = 20$ were considered in order to compare large amplitude cases which oscillate through $Re_c$, and smaller amplitude cases which are above $Re_c$ throughout the oscillation. The oscillating cylinder cases were computed for a total time record of twelve forcing periods.

Before proceeding to provide theoretical underpinnings for the numerical Koopman mode results using simplified normal form mathematical models, the reduced-order normal form approximations presented in Section 4 are verified by comparing with full-order CFD solutions. To demonstrate the concepts associated with dynamics-of-observables, we select the integrated transverse force coefficient on the cylinder, $c_y$, as the observable of interest since it is a convenient, and commonly used, representation of cylinder wake dynamics, e.g. (Cetiner & Rockwell 2001; Perdikaris *et al.* 2009),

$$\mathbf{g}(t, \mathbf{z}_0) = c_y(t). \tag{5.1}$$

Using the methodology outlined by Sreenivasan *et al.* (1987), explicit functions for the normal form coefficients, $\lambda_1$ and $\beta$, expressed in terms of the bifurcation parameter $\mu = (Re - Re_c)\nu/D^2$ are estimated from the stationary cylinder CFD solutions. The following expressions were used:

$$\lambda_1 = 0.17\mu + i\left(38.6\nu/D^2 + 0.7\mu\right), \tag{5.2}$$

$$\Re[\beta] = -0.2\mu/(c_{y,max})^2; \Im[\beta] = -3\Re[\beta]. \tag{5.3}$$

Spectral and time-signal comparisons between normal form theory and CFD results are presented in Figs. 1 and 2 for $f << f_0$. For simplicity, it was assumed that $Q_I = 0$ since $\omega_0 + \beta_I r^2 >> Q_I$ for the range of parameters that were considered. The leading order normal form approximations accurately capture the spectral broadening exhibited by the CFD solutions as oscillation amplitude is increased.

The transverse force time-signal comparisons corresponding to Fig. 1 are provided in Fig. 2. The similarities between full-order and approximate time-signals further illustrate the excellent agreement between the normal forms based on just one mode. The accuracy of the normal form approximations derived from center manifold reductions support the finding that using the unforced bifurcation mode as the basis can lead to an accurate first-order approximation of a forced Hopf bifurcation system. So while the broad spectral content associated with the CFD would indicate a complicated high-dimensional system, the 'complexity' can be simplified quite nicely into a low-order representation when

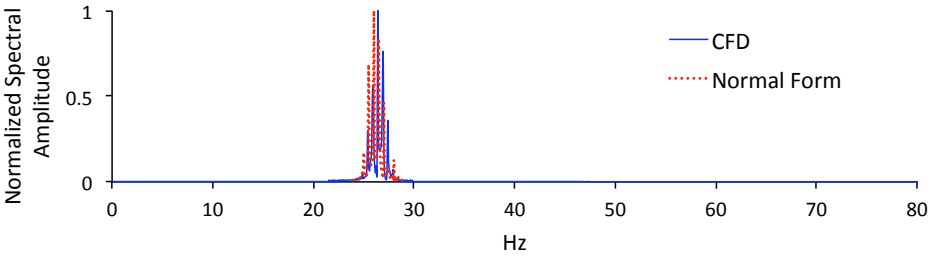


(a) $Re_q = 1$

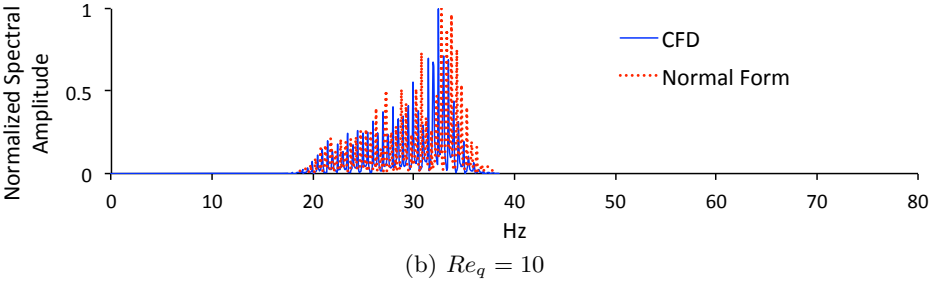


(b) $Re_q = 10$

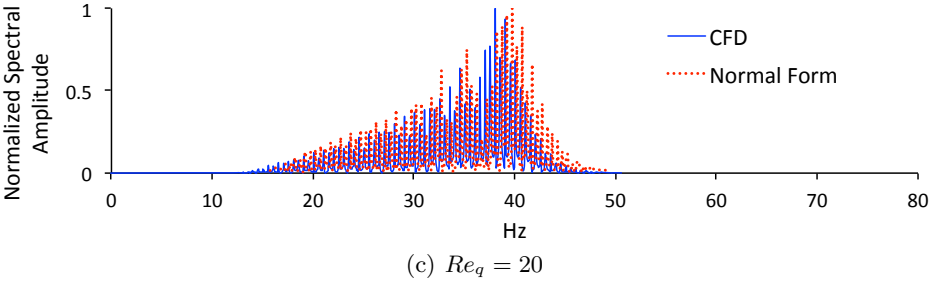


(c) $Re_q = 20$

FIGURE 1. Transverse force spectra for $f = 0.5$ Hz oscillating cylinder cases at various oscillation amplitudes for CFD and normal form solutions.

viewed from the correct perspective; in this case, the appropriate perspective is a basis spanned by the unforced Koopman bifurcation mode.

By proceeding with the full normal form simplifications using assumptions on $f$, we are able to show explicitly that $f << f_0$ is a necessary condition for leading order forcing effects to appear in the differential equation, and thus other scenarios for $f$ are precluded from inducing spectral broadening or chaos as a leading order phenomena spanned by the wake shedding mode. CFD and normal form results for a case when $f = f_0$ are contrasted with the $f << f_0$ case in Fig. 3.

Finally, we use normal form theory to demonstrate the importance of the dynamics-of-observables formalism that leads to a bi-linear structure of forcing/excitation terms when $\mathbf{g}$ is a nonlinear function of $\mathbf{z}$; see (4.4). Without undertaking the formal development in Section 4, one may be tempted to treat the effects of $\mathbf{u}$ by adding a simple harmonic forcing term to the unforced normal form equation, i.e.

$$\dot{\eta} = \lambda_1(\mu)\eta + \beta(\mu)\eta^2\bar{\eta} - iQ(\zeta - \bar{\zeta}), \tag{5.4}$$

rather than the correct bi-linear parametric excitation appearing in the normal form we derived. Similar analogies have been suggested to describe oscillating cylinder wake

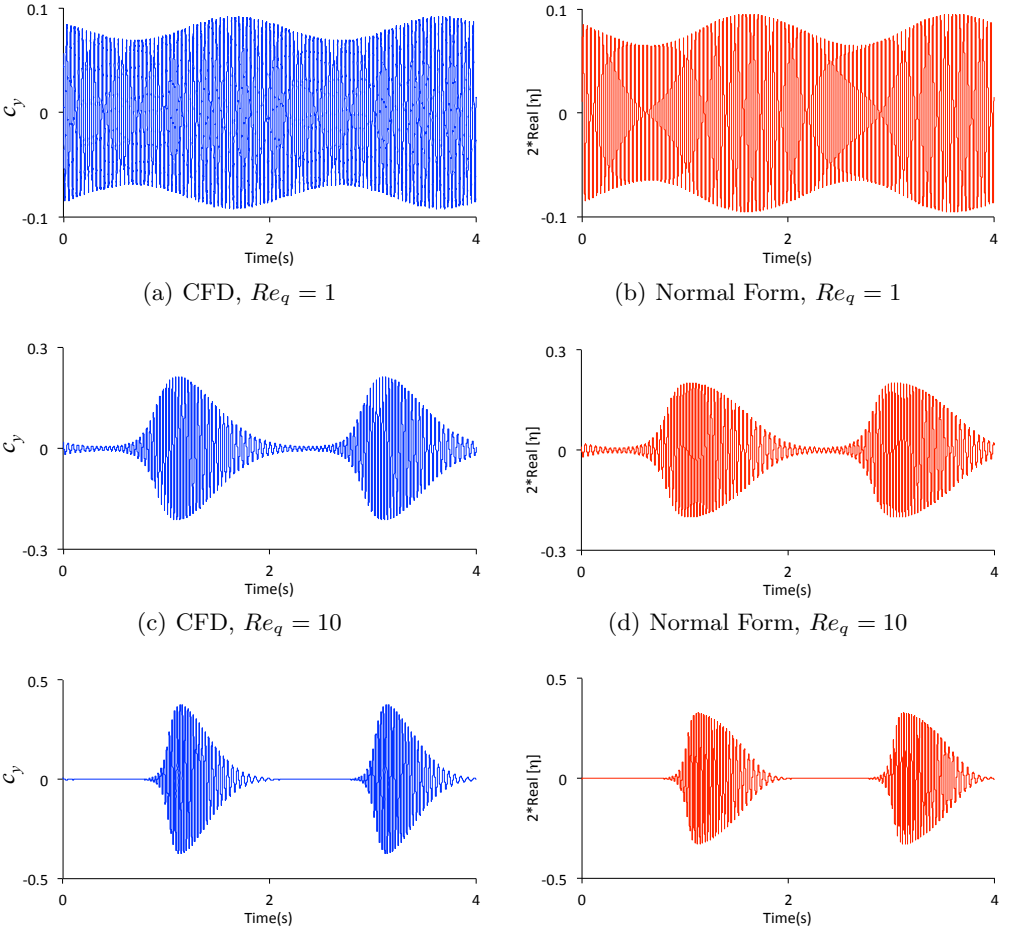


(a) CFD, $Re_q = 1$ (b) Normal Form, $Re_q = 1$

(c) CFD, $Re_q = 10$ (d) Normal Form, $Re_q = 10$

(e) CFD, $Re_q = 20$ (f) Normal Form, $Re_q = 20$

FIGURE 2. Transverse force coefficient time signals for $f = 0.5$ Hz oscillating cylinder cases at various oscillation amplitudes for CFD and normal form solutions.

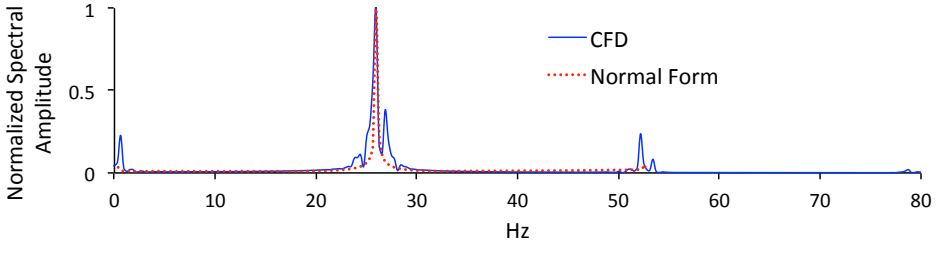


FIGURE 3. Transverse force spectra for $f = f_0 = 26.4$ Hz, $Re_q = 10$ oscillating cylinder case; normal form solutions based on (2.5).

dynamics, e.g. Provansal *et al.* (1987). However, as shown in this study, such an approach is only valid when $\mathbf{g}$ is a linear function of $\mathbf{z}$. For the more general dynamics-of-observables case, (5.4) is incorrect. In essence, the additive forcing is appropriate when considering the system states $\mathbf{z}$ as the observable of interest, while the parametric system is appropriate

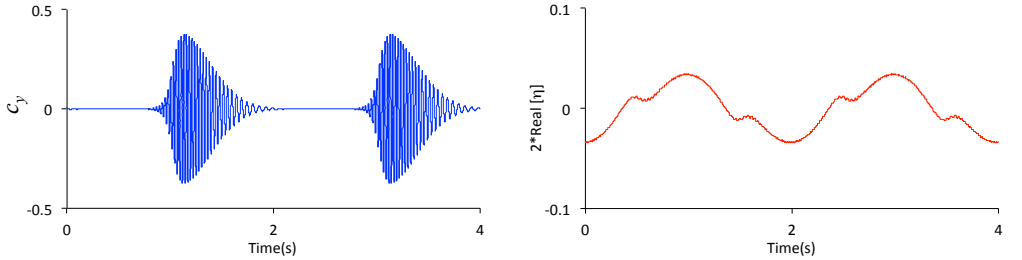


(a) CFD, $Re_q = 10$




(b) Normal form (5.4), $Re_q = 10$

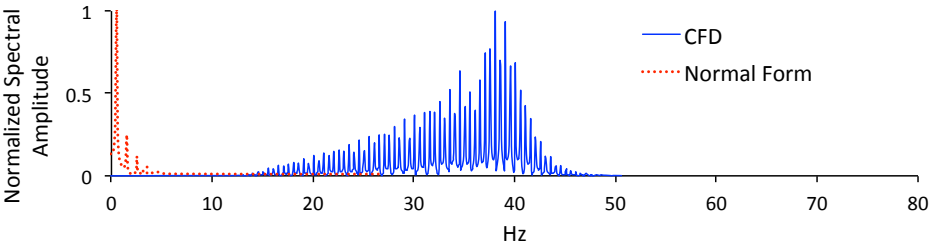


(c) Spectra

FIGURE 4. Transverse force coefficients for (a) CFD and (b) normal form with additive forcing term for a $f = 0.5$ Hz oscillating cylinder case; (c) corresponding spectral content.

for the dynamics of nonlinear functions of $\mathbf{z}$, such as force coefficients. To illustrate this, we reconsider the oscillating cylinder case for $f = 0.5$ Hz and $Re_q = 10$. Except, we now compare with the incorrect additive normal from (5.4), instead of the correct parametrically excited normal form whose solutions are shown in Figs. 1(b) and 2(d). From Fig. 4, it is clear that adding the forcing term to the unforced normal form equation in an ad hoc manner will lead to incorrect results when considering dynamics of a generic observable. This finding has significant implications for development of control strategies based on reduced-order models of observables since the proper way to introduce control inputs will be through bi-linear terms. The dynamics-of-observables approach can be viewed as a generalization of the additive normal form approaches, e.g. (Vance *et al.* 1989; Tsarouhas & Ross 1987, 1988; Gabale & Sinha 2009), since the correct normal form structure would be recovered if the observable of interest is a linear function of the underlying state $\mathbf{z}$. It is also worth noting that while parametrically excited Hopf bifurcation studies such as Bajaj (1986) include a bi-linear term, resonant phenomena (e.g. $f \sim 2f_0$) have typically been studied. In contrast, the dynamics of (4.14,4.15) for $f << f_0$ have, to the best of our knowledge, not been presented previously.

Having verified the two-dimensional reduced order normal form equations with respect to the full-order CFD solutions, we now proceed with determining the underlying nature of the spectral broadening that can manifest in the wake dynamics when $f << f_0$; i.e. are the dynamics quasi-periodic, chaotic, or something else? First, it is useful to visualize the attractor in state space. From Fig. 2, it appears that the trajectories pass near $r = |\eta| = 0$ as the oscillatory forcing amplitude $Re_q$ is increased. This is confirmed in Fig. 5.

How closely the attractor passes near $r = 0$ is a critical delineator between classical quasi-periodic dynamics and what we will later define as *Quasi-Periodic Intermittency*. This can be shown analytically by considering (4.14) which is decoupled from $\theta$. When

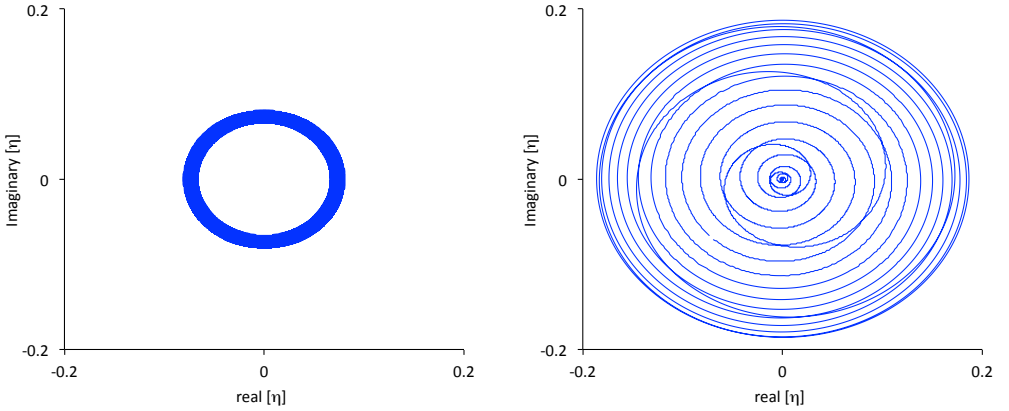


(a) $Re_q = 1$ (b) $Re_q = 20$

FIGURE 5. Normal form state space trajectories for one period corresponding to the forcing frequency $f$.

$r$ is sufficiently small, $\beta_R r^3 << (\sigma + 2Q_R \sin\omega_f t)\, r$, leading to

$$\dot{r} = (\sigma + 2Q_R \sin\omega_f t)\, r. \tag{5.5}$$

If $\beta_R r^3 << (\sigma + 2Q_R \sin\omega_f t^*)\, r$ at some time $t = t^*$, then the solution to (5.5) at $t = t^* + \Delta t$ is

$$r(t^* + \Delta t) = r(t^*) e^{\lambda_L \Delta t} \tag{5.6}$$

where

$$\lambda_L = \sigma + 2Q_R \left(\sin\omega_f t^* + \omega_f \Delta t \cos\omega_f t^*\right) \tag{5.7}$$

and the approximation $\sin\omega_f(t^* + \Delta t) \approx \sin\omega_f t^* + \omega_f \Delta t \cos\omega_f t^*$ has been used. Now we consider the evolution of two trajectories: the first $r_1(t^* + \Delta t)$ which is the solution beginning from $r(t^*)$, and the second $r_2(t^* + \Delta t)$ beginning from a perturbed initial condition $r(t^*) + \delta_0$. After substituting these initial conditions into (5.6), it is easy to show that the separation between the two trajectories, $\delta_r(t^* + \Delta t) \equiv r_2(t^* + \Delta t) - r_1(t^* + \Delta t)$, is

$$\delta_r(t^* + \Delta t) = \delta_0 e^{\lambda_L \Delta t}. \tag{5.8}$$

Furthermore, if $\dot{r} > 0$, then $\lambda_L > 0$. Therefore, the separation between the trajectories exponentially diverges for finite time when $\dot{r} > 0$, until $r$ increases sufficiently for $\beta_R r^3$ to become significant. This behavior is consistent with chaos since the difference between two nearby trajectories on the attractor exponentially diverges. In this context, $\lambda_L$ in (5.8) can be interpreted as a finite time Lyapunov exponent. Note that the system is only susceptible to exponential divergence of nearby trajectories at points on the attractor corresponding to small $r$ and $\dot{r} > 0$. The exponential divergence of nearby trajectories is illustrated in Fig. 6(a) where the two trajectories diverge as they spiral radially outwards ($\dot{r} > 0$) until reaching a sufficiently large value of $r$. In Fig. 6(a), the deviating trajectories are shown after 1000 forcing periods from the initial instant at which perturbation is introduced. Even though the system was only perturbed at one instant in time, the two trajectories will differ for all time due to the periodic occurrence of exponential divergence. Thus, the system exhibits the sensitive dependence on initial conditions on the attractor typically associated with chaotic systems. We have verified (not shown) that introducing similar perturbations elsewhere on the attractor away from small $r$,

or for smaller forcing amplitudes, will not induce exponential divergence and the two nearby trajectories will eventually coalesce and become indistinguishable after sufficient time from the initial perturbation.

The development of the finite time Lyapunov exponent as the number of iterations is increased is shown in Fig. 6(b). Although the system exhibits the classically chaotic feature of sensitive dependance on initial conditions for some points on the attractor, the Lyapunov exponent approaches 0 as $t \to \infty$. So in contrast to classically chaotic systems, the Lyapunov exponent is not positive over infinite time. Instead, as shown in the Fig. 6(b) inset, the divergence of nearby trajectories for $Re_q = 20$ is maintained for all time due to transiently positive finite time Lyapunov exponents as the system periodically passes by $r = 0$. For systems that do not pass near $r = 0$, as shown for the $Re_q = 1$ case in Fig. 6(b), the Lyapunov exponent never becomes positive even within finite time windows.

The effects of forcing amplitude on the susceptibility to exponential divergence over finite time is shown in Fig. 7, where the critical parameter for exponential divergence is

$$A = \frac{\beta_R r_{\min}^2}{(\sigma + 2Q_R \sin \omega_f t_{\min})} \tag{5.9}$$

in which $r_{\min}$ is the minimum value of $r(t)$ and $t_{\min}$ is the time at which $r_{\min}$ occurs. The horizontal line in Fig. 7 indicates when $A << 1$ and the system is sensitive to perturbation at certain points on the attractor. Note that the value of $10^{-3}$ was chosen arbitrarily as a small value for illustrative purposes. It is clear from Fig. 7 that the oscillatory forcing amplitude must be sufficiently large to drive the system near the fixed point. If $2Q_R$ is not $\geqslant \sigma$, then the system will never decay (although it will saturate due to the cubic term). As a result, $2Q_R \geqslant \sigma$ is a condition on the amplitude that is required for finite time exponential divergence to be possible. Otherwise, such behavior can be ruled out *a priori*. For $Re_q = 20$, $r_{\min} \sim \mathcal{O}(1e^{-8})$. Therefore, for larger oscillatory Reynolds numbers, the dynamics for the transverse force coefficient $c_y$ would have finite-time exponential divergence under realistic experimental conditions since very small perturbations (or lack of measurement precision for small numbers) are realities.

Interestingly, the system also exhibits quasi-periodic characteristics even after transitioning to exponential divergence for sufficient forcing amplitude. As shown in Fig. 8(a), the normal form solution corresponding to $Re_q = 20$ exhibits a discrete spectrum, as opposed to a continuous spectrum conventionally associated with chaos. The corresponding Poincaré section is shown in Fig. 8(b). The Poincaré section points are obtained by recording solutions at integer multiples of the forcing period $1/f$. The intersection points fill in a curve in the Poincaré plane, i.e. a drift ring, which is a clear indication of quasi-periodic dynamics (Hilborn 1994). Due to the described nature of this physical phenomenon - featuring finite-time exponential divergence, associated with the bursts shown in Fig. 2e, and quasi-periodic dynamics - we call it the Quasi-Periodic Intermittency.

Further insight can be gained by viewing a three-dimensional representation of the Quasi-Periodic Intermittency attractor obtained by plotting in toroidal coordinates, which is a common approach to visuaizing quasi-periodic and multi-scale behavior – see Section 4.7 of (Hilborn 1994) for example. In Fig. 9, the slower forcing scale (i.e. $f$) is represented by rotation around the larger diameter of the torus. It can be observed that the radial growth/decay (i.e. $\dot{r}$) corresponds to rotation around the torus, which is consistent with the fact that the forcing term manifests as a parametric excitation of the bifurcation parameter. Similarly, rotation around the cross-section (i.e. $\dot{\theta}$) corresponds to

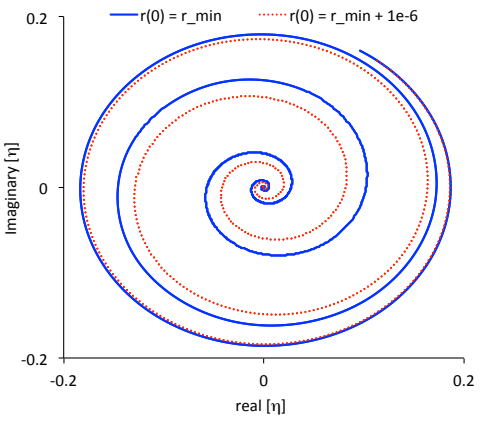


(a) Comparison of trajectories after perturbation

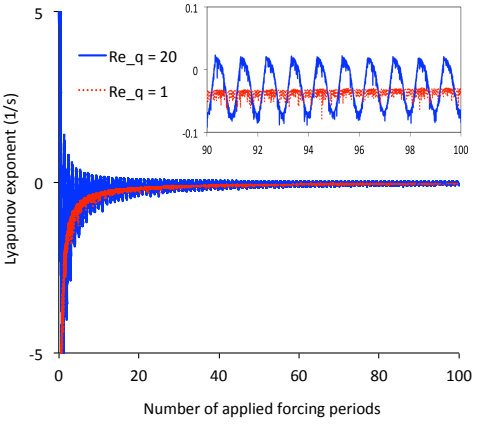


(b) Finite time Lyapunov exponents

FIGURE 6. (a) Comparison of state space trajectories beginning from perturbed initial conditions on the attractor in the regime where $\beta_R r^3 << (\sigma + 2Q_R \sin\omega_f t)\, r$ for $Re_q = 20$; note that the plot corresponds to 1000 forcing periods after the initial perturbation and only the portions of the trajectories corresponding to $\dot{r} > 0$ are shown for clarity. (b) The development of the finite time Lyapunov exponent for $Re_q = 20$ and $Re_q = 1$ over 100 forcing periods; the inset shows a zoomed in view.

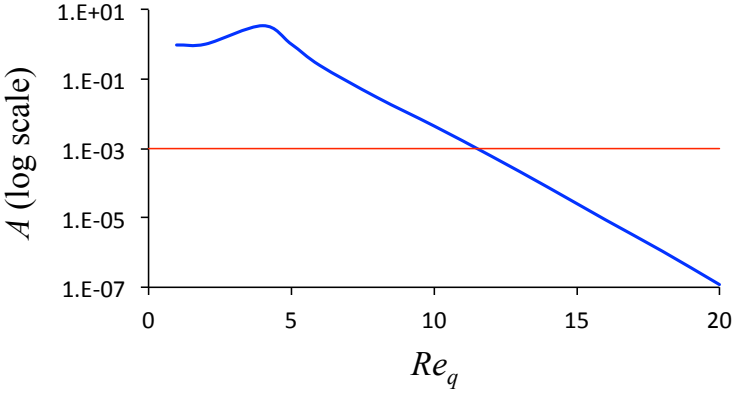


FIGURE 7. Variation of the critical parameter delineating the onset of chaos, $A$, with oscillatory Reynolds number amplitude.

the faster natural frequency $f_0$. Note that if one were to unfold the torus in Fig. 9 into a cylinder, the cross-sectional view of the cylinder would resemble Fig. 5(b).

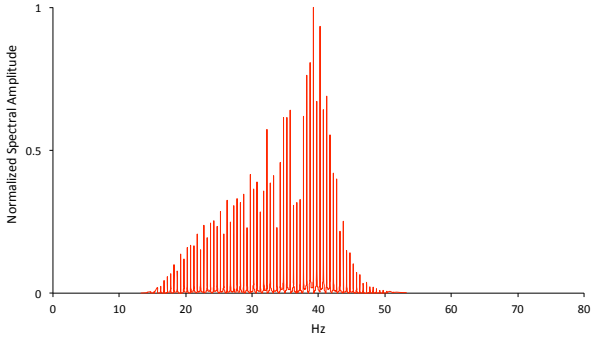


(a) Normal form spectrum

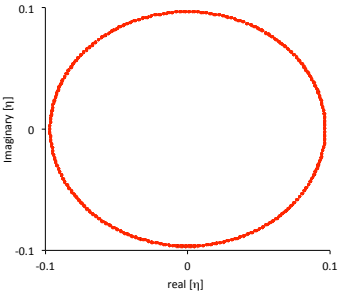


(b) Poincaré section

FIGURE 8. Discrete spectrum (a), and Poincaré section (b) corresponding to the normal form solution for $Re_q = 20$; both are computed from 1000 periods of forcing frequency $f = 0.5$ Hz.

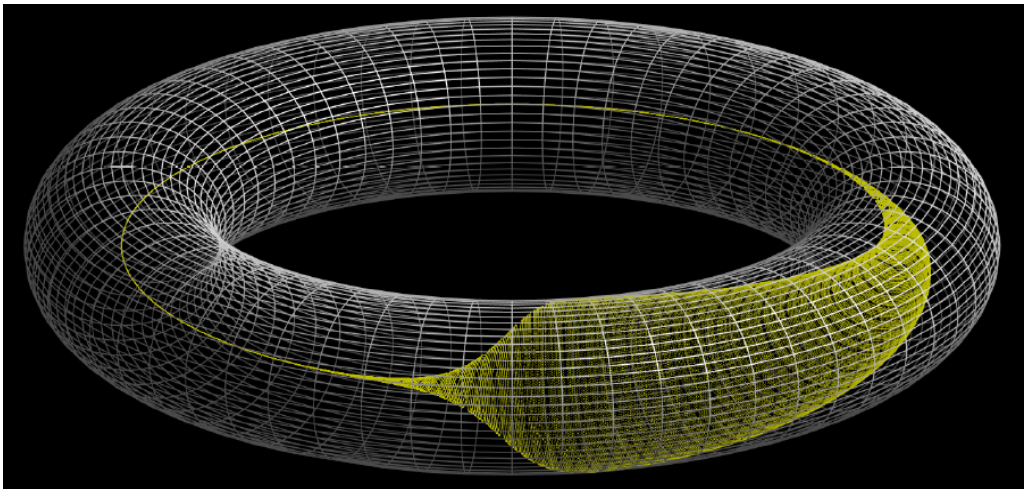

FIGURE 9. The Quasi-Periodic Intermittency attractor (yellow) plotted on the torus. The toroidal grid (grey) is shown for reference. Rotation around the large diameter of the torus corresponds to the radial growth/decay that occurs over the slow forcing frequency, while rotation around the smaller diameter (i.e. phase velocity as the attractor spins around cross sections of the torus) correspond to the faster natural frequency of the system. The figure corresponds to $Re_q = 20$ and 24 periods of motion corresponding to the forcing frequency $f$.

## 6. POD and KMD

We also performed the analysis and comparison between KMD and POD results applied to the considered above cases of stationary cylinder and all oscillating cylinder cases. Let us consider the oscillating cylinder case for Re=10. In Fig. 10 we show the energy, in Fig. 11 we show the coefficients of mode 1 and their spectrum, in Fig. 12 we show mode 1. The matrix showing the magnitude of inner products between the modes of significance in this case is given in Fig. 13. By using the obtained results, we can show that POD may smudge the modes under certain conditions because it tracks energy, while Koopman modes will isolate features based on scale rather than energy.

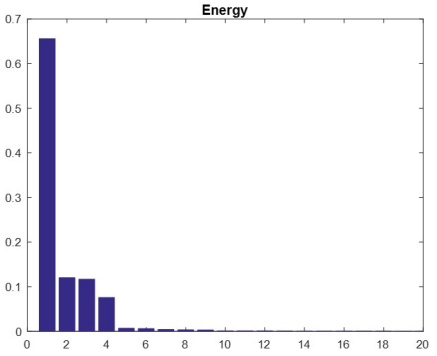


FIGURE 10. Energy

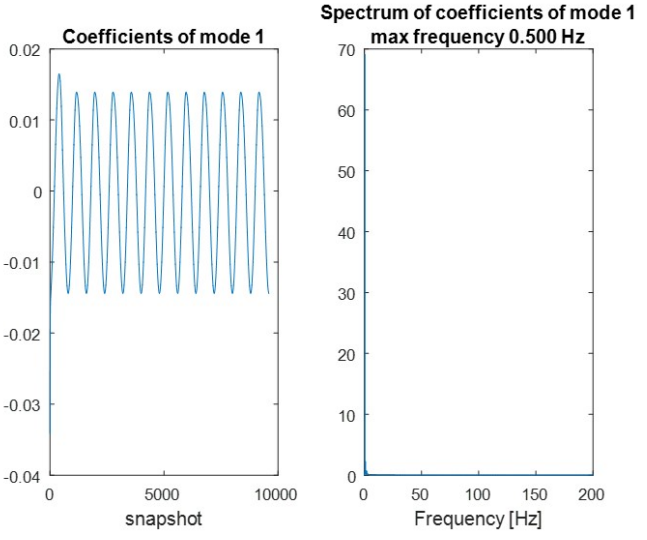


FIGURE 11. Coefficients of Mode 1

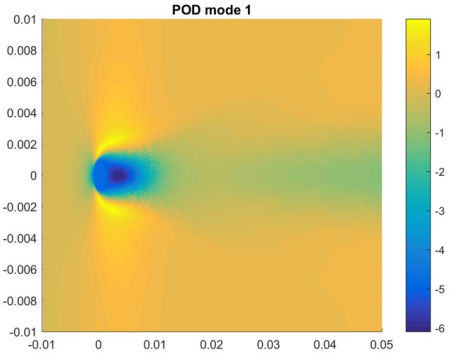


FIGURE 12. POD Mode 1

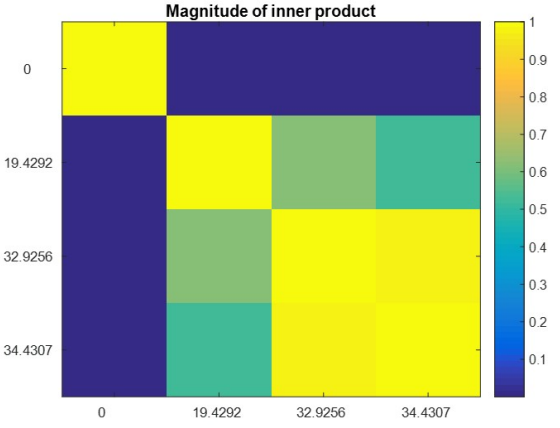


FIGURE 13. Ortogonality Matrix

## 7. Normal Form Control

We also worked on the normal form control question. The fixed points of the normal form equation and their stability are potentially of interest for control applications. Consider the integrated force coefficient magnitude equation:

$$\dot{r} = \sigma(\mu)r + \beta_R(\mu)r^3 + 2rQ_R\sin(\omega_f t) \tag{7.1}$$

which with its coefficients explicitly written out is:

$$\dot{r} = (0.17\mu)r + \left(\frac{-0.2\mu}{c_{y,max}^2}\right)r^3 + \left(\frac{-3q}{2}\right)r\sin(\omega_f t) \tag{7.2}$$

where $\mu = [Re_0 - Re_c - Re_q\sin(\omega_f t)](\frac{\nu}{D^2})$, $D$ is the cylinder radius, $Re_0$ is the oncoming freestream Reynolds number, $Re_c$ is the von Kármán vortex instability Reynolds number, and $Re_q$ is defined by $Re = Re_0 - Re_q *$forcing. Other variables are the streamwise velocity oscillation frequency $\omega_f$, the kinematic viscosity $\nu$, the forcing amplitude $q = \frac{Re_q\omega_f}{2D}$, and the maximum value of integrated transverse force coefficient on the cylinder $c_{y,max}$.

The fixed points are at $r = 0$ and

$$r = \pm\sqrt{\frac{\left[0.17 + \frac{3q}{2Re_q(\frac{\nu}{D^2})}\right]\mu - \frac{3q(Re_0 - Re_c)}{2Re_q}}{\frac{0.2}{c_{y,max}^2}\mu}} \tag{7.3}$$

where the stability of the fixed points depends on the time-dependent value of $\mu$.

The fixed point at the origin can be stabilized by adding a linear term to $\dot{r}$:

$$\dot{r}_{stable,origin} = \dot{r}_{original} - \left[0.17(Re_0 - Re_c + Re_q)\left(\frac{\nu}{D^2}\right) + \frac{3q}{2}\right]r \tag{7.4}$$

and the non-zero fixed points, when they exist, can also be stabilized by adding a linear term to $\dot{r}$:

$$\dot{r}_{stable,non-zero} = \dot{r}_{original} + 2\left[0.17(Re_0 - Re_c + Re_q)\left(\frac{\nu}{D^2}\right) - 9q\right]r \tag{7.5}$$

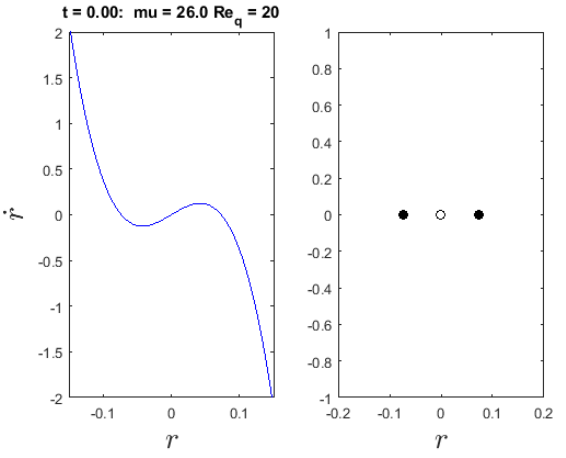


FIGURE 14. Original $\dot{r}$ at $t = 0$ seconds. The origin is unstable and the non-zero fixed points are stable.

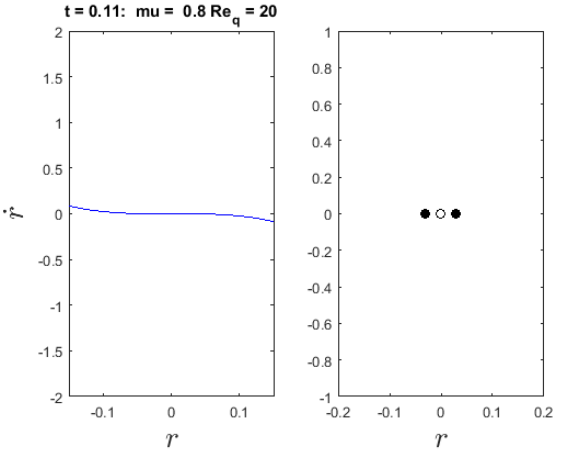


FIGURE 15. Original $\dot{r}$ at $t = 0.11$ seconds. The origin is unstable and the stable non-zero fixed points are approaching the origin.

## 8. Conclusions

We utilized Koopman decompositions of cylinder flow-fields due to prescribed streamwise velocity oscillations superimposed on a steady flow component to gain understanding of dynamics for the separation-of-scale regime $f << f_0$. We derived the effect of forcing from a dynamics-of-observables perspective where it is shown that oscillating the streamwise Reynolds number is equivalent to exciting the Hopf bifurcation parameter. We described a center-manifold reduction using Koopman modes, followed by further simplification of nonlinearities using normal form theory. Finally, we presented the results which establish the accuracy of the reduced-order normal form mathematical models, and provide theoretically grounded evidence of a new dynamical systems phenomena that occurs in the $f << f_0$ regime. We also worked on the comparison between the POD and KMD analysis and the normal form equation control.

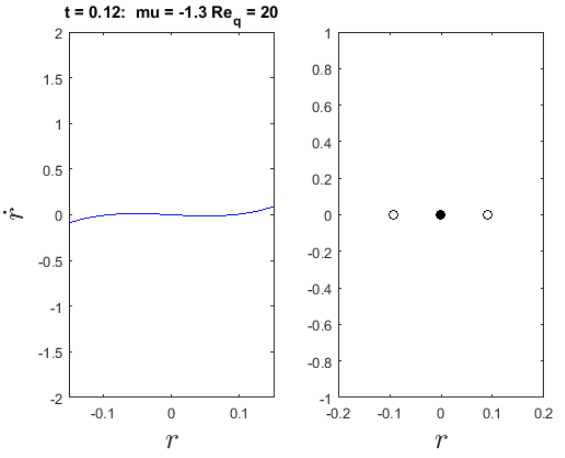


FIGURE 16. Original $\dot{r}$ at $t = 0.12$ seconds. The origin is now stable and the non-zero fixed points unstable.

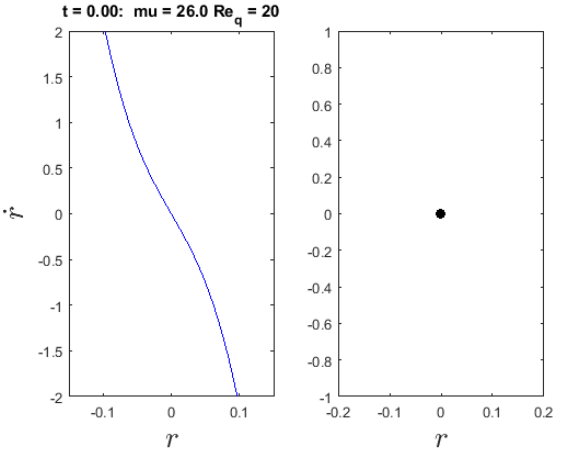


FIGURE 17. $\dot{r}_{stable,origin}$ at $t = 0$ seconds. The origin is stable and the non-zero fixed points do not exist.

## REFERENCES


BAGHERI, S. 2013 Koopman-mode decomposition of the cylinder wake. *Journal of Fluid Mechanics* **726**, 596–623.

BAJAJ, A.K. 1986 Resonant parametric perturbations of the Hopf bifurcation. *Journal of Mathematical Analysis and Applications* **115**, 214–224.

CETINER, O. & ROCKWELL, D. 2001 Streamwise oscillations of a cylinder in steady current. part 1. locked-on states of vortex formation and loading. *Journal of Fluid Mechanics* **427**, 1–28.

GABALE, A. P. & SINHA, S. C. 2009 A direct analysis of nonlinear systems with external periodic excitations via normal forms. *Nonlinear Dynamics* **55** (1), 79–93.

GUCKENHEIMER, J. & HOLMES, P. 1983 *Nonlinear Oscillations, Dynamical Systems, and Bifurcations of Vector Fields*. Springer.

HILBORN, R.C. 1994 *Chaos and Nonlinear Dynamics: An Introduction for Scientists and Engineers*. Oxford University Press.

KOOPMAN, B.O. 1931 Hamiltonian systems and transformation in Hilbert space. *Proceedings of the National Academy of Sciences of the United States of America* **17** (5), 315.

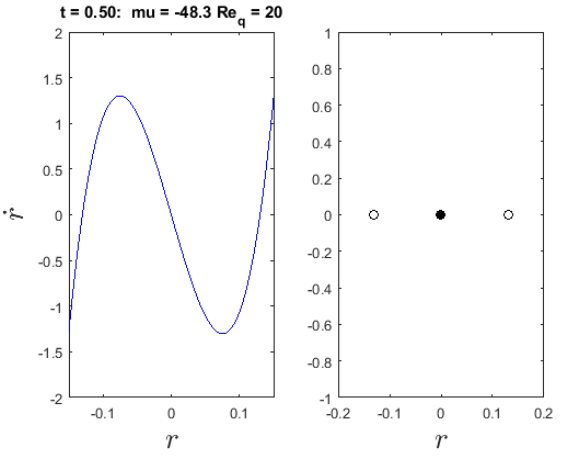


FIGURE 18. $\dot{r}_{stable,origin}$ at $t = 50$ seconds. The origin is stable and the non-zero fixed points are unstable when they exist.

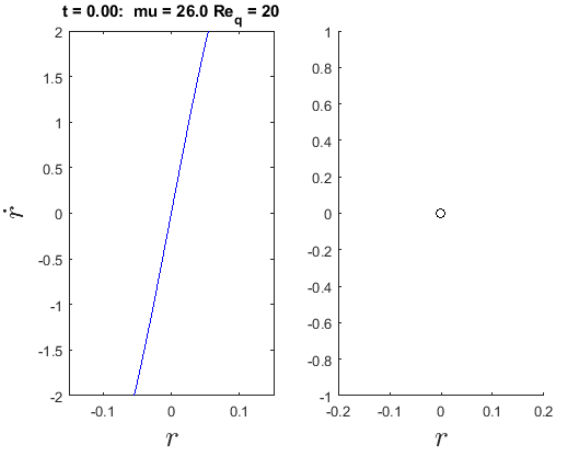


FIGURE 19. $\dot{r}_{stable,non-zero}$ at $t = 0$ seconds. The origin is unstable and the non-zero fixed points do not exist.


LEONTINI, J. S., JACONO, D. L. & THOMPSON, M. C. 2013 Wake states and frequency selection of a streamwise oscillating cylinder. *Journal of Fluid Mechanics* **730**, 162–192.

LIN, K. K. & YOUNG, L. S. 2008 Shear-induced chaos. *Nonlinearity* **21**, 899–922.

MEZIĆ, I. 2005 Spectral properties of dynamical systems, model reduction and decompositions. *Nonlinear Dynamics* **41** (1), 309–325.

MEZIĆ, I. 2013 Analysis of fluid flows via spectral properties of the Koopman operator. *Annual Reviews of Fluid Mechanics* **45**, 357–378.

NAYFEH, A. H. 2011 *The Method of Normal Forms*. John Wiley and Sons.

PERDIKARIS, P.G., KAIKTSIS, L. & TRIANTAFYLLOU, G.S. 2009 Chaos in a cylinder wake due to forcing at the Strouhal frequency. *Physics of Fluids* **21**.

PROVANSAL, M., MATHIS, C. & BOYER, L. 1987 Benard-von Kármán instability: Transient and forced regimes. *Journal of Fluid Mechanics* **182**, 1–22.

ROWLEY, C.W., MEZIĆ, I., BAGHERI, S., SCHLATTER, P. & HENNINGSON, D.S. 2009 Spectral analysis of nonlinear flows. *Journal of Fluid Mechanics* **641** (1), 115–127.

SCHMID, PETER & SESTERHENN, JOERN 2008 Dynamic mode decomposition of numerical and experimental data. 61st Annual Meeting of the APS Division of Fluid Dynamics.

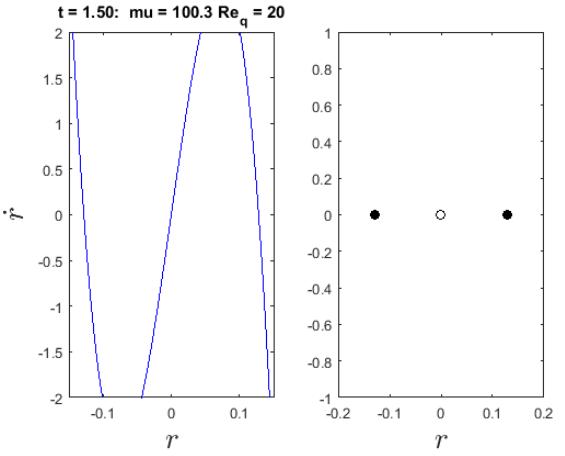


FIGURE 20. $\dot{r}_{stable,non-zero}$ at $t = 150$ seconds. The origin is unstable and the non-zero fixed points are stable when they exist.


SINGH, RK & MANHAS, JS 1993 *Composition operators on function spaces*. North Holland.

SREENIVASAN, K. R., STRYKOWSKI, P. J. & OLINGER, D. J. 1987 Hopf bifurcation, Landau equation and vortex shedding behind circular cylinders In Proc. Forum Unsteady Separation, ed. K. N. Ghia, 52.

SUSUKI, YOSHIHIKO & MEZIĆ, IGOR 2012 Nonlinear Koopman modes and a precursor to power system swing instabilities. *Power Systems, IEEE Transactions on* **27** (3), 1182–1191.

TSAROUHAS, G. E. & ROSS, J. 1987 Explicit solutions of normal form of driven oscillatory systems. *Journal of Chemical Physics* **87** (11), 6538–6543.

TSAROUHAS, G. E. & ROSS, J. 1988 Explicit solutions of normal form of driven oscillatory systems in entrainment bands. *Journal of Chemical Physics* **88** (9), 5715–5720.

VANCE, W., TSAROUHAS, G. & ROSS, J. 1989 Universal bifurcation structures of forced oscillators. *Progress of Theoretical Physics Supplement* **99**, 331–338.

WANG, Q. & YOUNG, L. S. 2003 Strange attractors in periodically-kicked limit cycles and hopf bifurcations. *Communications in Mathematical Physics* **240**, 509–529.

WIGGINS, S. 1990 *Introduction to Applied Nonlinear Dynamical Systems and Chaos*. Springer-Verlag.